Bayesian image restoration in Astronomy. Application to images of the recent collision of comet Shoemaker-Levy 9 with Jupiter.

R. Molina, J. Mateos, J. Abad, N. Pérez de la Blanca
Departamento de Ciencias de la Computación e I.A.
Universidad de Granada, 18071 Granada, España

A. Molina*, F. Moreno
Instituto de Astrofísica de Andalucía. C.S.I.C.
P.O. Box 3004, 18080 Granada, España
*Also at Dpto. de Física Aplicada, Univ. de Granada, España

Abstract

In this work we examine from simple to complex methods proposed within the Bayesian paradigm to perform image restoration in Astronomy. We shall start by describing the classical conditional and simultaneous autoregressions, then we shall move on to study how to incorporate smoothness constraints to the classical Richardson-Lucy restoration method and also examine how to modify the image scale and define prior models on other scales than the linear one. Finally, we shall compare those models on images of Jupiter after the impacts of the fragments of the comet Shoemaker-Levy 9 at two wavelengths.

1 Introduction

The distortion produced by the Earth's atmosphere on the observed light distribution of extended objects is the main problem for the spatial resolution in optical astronomy. The observed luminosity distribution of a distant object is the result of the two-dimensional convolution of the unknown light distribution with instrumental effects (telescope + detector) and, mainly, atmospheric distortion. All the processes that produce a blurred image can be represented by a point spread function, *psf*. In addition the collected image is degraded by noise produced by detectors and by the intrinsic discrete nature of light. A clear example of an effect produced by observational distortion is the change in the shape of the brightness profile in cores of elliptical galaxies and in bulges of spirals.

Modern detectors provide images of high signal-to-noise ratio and long dynamic range, facilitating the digital processing and the application of restoration methods to remove the seeing blur and enhance small features in the images. During recent years several techniques for the deconvolution of observational *psf*'s have been developed based on different algorithms, linear or non-linear; (see for instance [1], [2], [3], [4] and [5], see also [6] for a point of view of the restoration of astronomical images).

The spherical aberration of the Hubble Space Telescope (HST) optics has also led to an enormous interest in image restoration in the astronomical community. Even being the COSTAR corrective optics in place, image restoration has a role to play (see for instance [6] for an overview of the problem of restoring HST images, the proceedings [7] and [8] are probably the most important workshops on restoration of HST images held so far, and ST-ECF Newsletters for continuous references to deconvolution of HST images). So far, the most used method for restoration of HST images seems to be the Richardson-Lucy (R-L) method (see [9] and [4]), although maximum entropy methods, in particular the MemSys package [2], are also frequently used in the astronomical community.

In this paper we present a battery of Bayesian methods to deconvolve astronomical images in the presence of noise. The Bayesian paradigm is described in section 2. The models for the blurring and noise processes are discussed in section 3. Prior models for the deconvolution of galaxies and planets are described and justified in section 4. In section 5, algorithms to find the restoration are described. Finally, in section 6 a test of the performance of the restoration methods is carried out in real images by the application of the algorithms to high quality images of Jupiter acquired during the impact of comet Shoemaker-Levy 9 on Jupiter on July 1994.

2 Bayesian Paradigm

The philosophy within statistics known as Bayesian inference has a very long history. It is distinguished from the perhaps more familiar classical statistical ideas by using prior information about the images being studied.

Bayesian methods start with a prior distribution, a probability distribution over images $\mathbf{f}$, $p(\mathbf{f})$, (it is here that we incorporate information on the expected structure within an image), it is also necessary to specify the probability distribution $p(\mathbf{g}|\mathbf{f})$, of observed images $\mathbf{g}$ if $\mathbf{f}$ were the true image. The Bayesian paradigm dictates that inference about the true $\mathbf{f}$

should be based on $p(\mathbf{f}|\mathbf{g})$ given by

$$p(\mathbf{f}|\mathbf{g}) \propto p(\mathbf{f})p(\mathbf{g}|\mathbf{f})$$

To show just one restoration, it is common to choose the mode of this posterior distribution, that is to display the image $\hat{\mathbf{f}}$ which satisfies

$$\hat{\mathbf{f}} \text{ maximizes } p(\mathbf{f})p(\mathbf{g}|\mathbf{f})$$

This is known as the maximum a posteriori (MAP) estimate of $\mathbf{f}$.

Equivalently, we can choose $\hat{\mathbf{f}}$ to minimize

$$-\log p(\mathbf{g}|\mathbf{f}) - \log p(\mathbf{f}) \tag{1}$$

the first term in (1) is the familiar log likelihood of $\mathbf{f}$. The second term can be thought of as a roughness penalty, as images $\mathbf{f}$ which do not correspond to our prior conceptions will be assigned a small $p(\mathbf{f})$ and hence a large penalty.

In statistical physics it is common to define probabilities by the energy U of a system, so that

$$p(\mathbf{f}) \propto \exp[-\beta U(\mathbf{f})] \tag{2}$$

where β is $1/kT$, T being the temperature and k Boltzmann's constant. If we adopt this notation, $\hat{\mathbf{f}}$ minimizes

$$-\log \text{likelihood} + \beta U(\mathbf{f}) \tag{3}$$

We can recognize this as a Lagrangian form, so its solution is equivalent to solving

$$\max \text{ likelihood subject to energy} \leq \text{constraint}$$

and to

$$\min \text{ energy subject to likelihood} \geq \text{constraint}$$

which corresponds to the regularization approach to image restoration.

Many other deconvolution principles fit into one of these forms, in particular R-L restoration method ([4]) and maximum entropy methods ([1]).

Having described the Bayesian paradigm let us move on to examine the two ingredients of this paradigm, the observation process, $p(\mathbf{g}|\mathbf{f})$, and the prior model or image model, $p(\mathbf{f})$.

3 Observation Process

3.1 Blurring Process

The observed image $\mathbf{g}$ differs from $\mathbf{f}$ in having been blurred by atmospheric motion and also in the statistical noise present in the recording process. Theoretical and empirical studies (see [10] for references) suggest that the blurring function, h, can be approximated by

$$h(r) = (\beta/\pi R^2)[1 + (r/R)^2]^{-\beta} \tag{4}$$

where r is the distance to the pixel that receives the light and β and R depend on the atmospheric conditions of the night when the observation was taken. The form of h can be checked, and β and R calculated, because most images have true source points of light. Physical considerations yield the following expression for the observed image

$$\mathbf{g} = \mathbf{Df} + \varepsilon \tag{5}$$

where $\mathbf{D}$ is the blurring matrix calculated from the *psf* and ε is the error vector due to the observation, whose components are independent given $\mathbf{f}$ and their variance possibly depends on $(\mathbf{Df})_i$.

So, if $p = m \times n$ is the size of the image, the blurring process is described by $\mathbf{Df}$ where $\mathbf{f}$ is a $p \times 1$ vector and $\mathbf{D}$ is the $p \times p$ point spread matrix defining the systematic blur and assumed to be known.

Let us describe the noise models.

3.2 Noise Models

For the observed vector $\mathbf{g}$ we could assume the following normal distribution

$$\mathbf{g} \sim \mathcal{N}((\mathbf{Df}), \sigma_\varepsilon^2 \mathbf{I}) \tag{6}$$

which is probably the simplest model for the noise, although, as we shall see in the examples, it produces good restorations.

Let us now study a more realistic noise model for astronomical images. For each component i, $i = 1, 2, \ldots, m \times n$ of the observed vector $\mathbf{g}$, we could use a Poissonian model, thus obtaining

$$\mathbf{g}_i \sim \mathcal{P}((\mathbf{Df})_i)$$

This model can be approximated, at least for high brightness values, by the Gaussian distribution $\mathcal{N}((\mathbf{Df})_i, (\mathbf{Df})_i)$.

An alternative model would be to assume $\mathbf{g}_i = \lambda \mathbf{z}_i$ where $\mathbf{z}_i \sim \mathcal{P}(\mathbf{Df})_i$, this is the case in many images provided by the astronomers. For this model we could use the following Gaussian approximation

$$\mathbf{g}_i \sim \mathcal{N}((\mathbf{D}(\lambda \mathbf{f}))_i, \lambda(\mathbf{D}(\lambda \mathbf{f}))_i) \tag{7}$$

substituting $\lambda \mathbf{f}$ by $\mathbf{f}$, we would have

$$\mathbf{g}_i \sim \mathcal{N}((\mathbf{Df})_i, \lambda(\mathbf{Df})_i) \tag{8}$$

Finally, a model like

$$\mathbf{g}_i \sim \mathcal{P}((\mathbf{Df})_i) + \mathcal{N}(0, \sigma^2)$$

and the corresponding $\lambda \mathbf{z}_i + \mathcal{N}(0, \sigma^2)$, ([11]) can be approximated by normal distributions having the form $\mathcal{N}((\mathbf{Df})_i, a + b(\mathbf{Df})_i)$ for appropriate constants a and b.

Let us examine more deeply the Gaussian approximation. We have in this case,

$$-2 \log p(\mathbf{g}|\mathbf{f}) = \text{const} + \sum_i E_i^2 \tag{9}$$

with $E_i = [(\mathbf{g}_i - (\mathbf{Df}_i))/\sigma(\mathbf{Df}_i)]$, being $\sigma((\mathbf{Df})_i)$ the standard deviation, $\sqrt{a + b(\mathbf{Df})_i}$ in the noise model just described.

This Gaussian approximation allows the easy incorporation of robust statistics concepts to deal with detector errors ([10]). The idea is to downweigh observations which are far away from their means. Such values are given too much weight in (9). The squared term in E_i represents the number of standard deviations that $\mathbf{g}_i$ is away from its mean. In robust statistics $\sum_i E_i^2$ is replaced by $\rho(E_i)$ for a function ρ which penalizes extreme values less severely. A typical function ρ is the Huber's 'proposal 2' function defined by

$$\rho(x) = \begin{cases} x^2 & \text{for} \quad |x| \leq c \\ 2c|x| - c^2 & \text{for} \quad |x| > c \end{cases} \tag{10}$$

This is quadratic in the centre, but penalizes large deviations linearly rather than quadratically. Equivalently, observations E_i are downweighted if $|E_i|$ exceeds 2. In practice c is chosen at about 2, which downweighs only those observations more than two standard deviations away from their means.

4 Prior Models

Having studied the degradation model, let us now examine the image or prior models.

4.1 Linear Scale

The simplest model consists on working at linear scale. Consider an image with no stars but regions of smoothly varying luminosity. We then expect $\mathbf{f}_i \geq 0$ and $\mathbf{f}$ to be spatially smooth. In this case smoothness is modelled by spatial autoregressions ([12]).

The conditional autoregression (C.A.R.) model is defined by

$$p(\mathbf{f}) \propto \exp\left\{-\frac{1}{2\sigma_{\mathbf{f}}^2}\mathbf{f}^t(\mathbf{I} - \phi\mathbf{N})\mathbf{f}\right\}$$

where $\sigma_{\mathbf{f}}^2$ is the unknown prior variance, matrix $\mathbf{N}$ is such that $\mathbf{N}_{ij} = 1$ if cells i and j are spatial neighbours, (pixels at distance one), zero otherwise and scalar ϕ is just less than 0.25. The term $\mathbf{f}^t(\mathbf{I} - \phi\mathbf{N})\mathbf{f}$ represents in matrix notation the sum of squares of the values $\mathbf{f}_i$ minus ϕ times the sum of $\mathbf{f}_i\mathbf{f}_j$ for neighbouring pixels i and j.

The parameters can be interpreted by the following expressions describing the conditional distribution

$$\begin{aligned} E(\mathbf{f}_i \mid \mathbf{f}_j,\ j \neq i) &= \phi \sum_{j \text{ nhbr } i} \mathbf{f}_j \\ \text{var}(\mathbf{f}_i \mid \mathbf{f}_j,\ j \neq i) &= \sigma_{\mathbf{f}}^2 \end{aligned}$$

where the suffix 'j nhbr i' denotes the four neighbour pixels at distance one from pixel i. The parameter $\sigma_{\mathbf{f}}^2$ measures the smoothness of the 'true' image.

It is important to note that this model can be extended to incorporate a line process that removes smoothness constraints when pixels do not belong to the same region. To our

knowledge this method has only be applied to astronomical images when the object location is known ([13]).

4.2 Log Scale

Let us now modify the smoothness scale. The luminosity distribution of pure disk in a galaxy can be modeled by "the exponential law" written as

$$I(r) = I(0)\exp(-b_0 r) \tag{11}$$

Furthermore, the luminosity distribution of elliptical galaxies has been investigated by many astronomers, and several analytical functions have been proposed to model this distribution. Among others, the most commonly used is 'the $r^{1/4}$ law' proposed by de Vaucouleurs,

$$\log(I(r)/I_E) = -3.33[(r/r_E)^{1/4} - 1] \tag{12}$$

where r is the distance from the center of the galaxy and I_E and r_E are parameters which differ from galaxy to galaxy.

These results suggest that the luminosity of galaxies is most naturally considered on log scale. The smoothness of the luminosity was then modelled on log scale except for very small values of luminosity (see [10] and [14]).

We therefore examine the use of a C.A.R. prior for $\mathbf{y} = \ln(\mathbf{f} + \gamma\mathbf{1})$, where γ is a small constant. Then for the C.A.R. model on log scale and the Gaussian noise model we have

$$-2\ln P(\mathbf{y}|\mathbf{g}) = const + \frac{1}{\sigma_{\mathbf{y}}^2}\mathbf{y}^t(\mathbf{I} - \mathbf{C})\mathbf{y} + \frac{1}{\sigma_\varepsilon^2} \parallel \mathbf{g} - \mathbf{Df} \parallel^2,$$

as the expression to be minimized for $\mathbf{y}$, where $\sigma_{\mathbf{y}}^2$ is the variance of the image model for $\mathbf{y}$ and $\mathbf{C} = \phi\mathbf{N}$. It is very important to note that we are proposing an image model for $\mathbf{y}$ and then obtaining an estimate of the source image as $\hat{\mathbf{f}} = \exp[\hat{\mathbf{y}}] - \gamma\mathbf{1}$, where $\hat{\mathbf{y}}$ minimizes the previous equation.

4.3 Flat priors

Let us finally examine the prior model used in the R-L ([4] and [9]) restoration method. This method aims at maximizing $p(\mathbf{g}|\mathbf{f})$ when this conditional distribution is Poissonian. Under the Bayesian framework this is the same as maximizing the posterior distribution for the prior model $p(\mathbf{f}) = \text{const}$, together with the Poissonian noise model. The meaning of this prior is simple; all possible restorations have the same probability.

5 Algorithms

Having defined the prior and degradation models, let us move on to estimate the MAP. For the sizes of problem we have to consider, efficient algorithms are essential. Many of the algorithms proposed below are iterative, and we have found it essential to use a good starting point to avoid the need for more than a few iterations.

Our algorithms are all related, but each includes some of a range of extra features in either the prior or noise model.

5.1 C.A.R. image model and signal independent noise.

The simplest case is that of a C.A.R. model for $\mathbf{f}$ and a Gaussian noise model. Then $\hat{\mathbf{f}}$ minimizes

$$\frac{1}{2\sigma_\varepsilon^2} \parallel \mathbf{g} - \mathbf{D}\mathbf{f} \parallel^2 + \frac{1}{2\sigma_{\mathbf{f}}^2}\mathbf{f}^t(\mathbf{I}-\mathbf{C})\mathbf{f} \tag{13}$$

which is a quadratic function. Thus the unconstrained solution satisfies

$$(\mathbf{D}^t\mathbf{D} + \lambda\mathbf{I} - \lambda\mathbf{C})\mathbf{f} = \mathbf{D}^t\mathbf{g} \tag{14}$$

with $\lambda = \sigma_\varepsilon^2/\sigma_{\mathbf{f}}^2$. This equation can be solved, rather quickly, using Fourier transform, assuming a toroidal correction. It is clear that the non negative constraint is not incorporated here, however, the method can be modified to produce non negative solutions ([10]). This model will be noted CARN (C.A.R. prior + Normal noise) in our examples.

5.2 C.A.R. model and Poisson noise

Following the R-L method, which, as we have said, corresponds to maximum a posteriori estimation with a uniform image prior, we seek to find

$$\mathbf{f}_{RL} = arg\max_{\mathbf{f}}\{\prod_{i=1}^{p} \exp\left[-(\mathbf{D}\mathbf{f})_i\right][(\mathbf{D}\mathbf{f})_i]^{\mathbf{g}_i}/\mathbf{g}_i!\} \tag{15}$$

Applying logarithms and differentiating with respect to $\mathbf{f}$ we obtain the following equation

$$\mathbf{D}^t(\mathbf{g}/\mathbf{D}\mathbf{f}_{RL}) = \mathbf{1} \tag{16}$$

where we have assumed that $\mathbf{D}^t\mathbf{1} = \mathbf{1}$. To solve (16) Lucy uses the iterative scheme

$$\mathbf{f}^{j+1} = \mathrm{Diag}(\mathbf{f}^j)[\mathbf{D}^t(\mathbf{g}/\mathbf{D}\mathbf{f}^j)]$$

where j denotes iteration and $\mathrm{Diag}(\mathbf{f}^i)$ is a diagonal matrix with diagonal entries $\mathbf{f}_i^j$. This iterative scheme is justified as an iterative scheme derived from EM principles. However, it can also be obtained by multiplying, component wise, both sides of (16) by $\mathbf{f}$.

Let us now assume that we want to impose smoothness constraints on the solution by using a C.A.R. prior model, we have

$$p(\mathbf{f}|\mathbf{g}) \propto \exp[-\frac{1}{2\sigma_{\mathbf{f}}^2}\mathbf{f}^t(\mathbf{I}-\mathbf{C})\mathbf{f}] \prod_{i=1}^{p} \exp\left[-(\mathbf{D}\mathbf{f})_i\right][(\mathbf{D}\mathbf{f})_i]^{\mathbf{g}_i}/\mathbf{g}_i! \tag{17}$$

Differentiating $-\log p(\mathbf{f}|\mathbf{g})$ with respect to $\mathbf{f}$ we obtain

$$\frac{1}{\sigma_{\mathbf{f}}^2}(\mathbf{I}-\mathbf{C})\mathbf{f} + \mathbf{1} - \mathbf{D}^t(\mathbf{g}/\mathbf{D}\mathbf{f}) = 0$$

or

$$\mathbf{f} + \sigma_{\mathbf{f}}^2 \mathbf{1} = \mathbf{C}\mathbf{f} + \sigma_{\mathbf{f}}^2 \mathbf{D}^t(\mathbf{g}/\mathbf{D}\mathbf{f}) \tag{18}$$

multiplying, component wise, both sides of (18) by $\mathbf{f}$ we obtain the following iterative scheme

$$\mathbf{f}^{j+1} = \mathrm{Diag}(\mu^j)\mathbf{C}\mathbf{f}^j + (\mathbf{I} - \mathrm{Diag}(\mu^j))\mathrm{Diag}(\mathbf{f}^j)\mathbf{D}^t(\mathbf{g}/\mathbf{D}\mathbf{f}^j) \tag{19}$$

where j denotes iteration and $\mathrm{Diag}(\mu^j)$ is a diagonal matrix with diagonal entries $\mathbf{f}_i^j/(\mathbf{f}_i^j + \sigma_{\mathbf{f}}^2)$.

It is interesting to note that $\mu_i^j = 0, \forall i, j$ corresponds to the classical R-L restoration method. This model will be noted CARP (C.A.R. prior + Poisson noise) in our examples.

5.3 Log scale C.A.R. image model and signal independent noise

When $\mathbf{y}$ is used instead of $\mathbf{f}$, to obtain the restoration we minimize

$$\frac{1}{\sigma_{\mathbf{y}}^2}(\mathbf{I} - \mathbf{C})\mathbf{y} + \frac{1}{\varepsilon^2} \parallel \mathbf{g} - \mathbf{D}\mathbf{f} \parallel^2$$

Differentiating this equation with respect to $\mathbf{y}$ we obtain that the solution, $\hat{\mathbf{y}}$, satisfies

$$\frac{1}{\sigma_{\mathbf{y}}^2}(\mathbf{I} - \mathbf{C})\mathbf{y} - \frac{1}{\sigma_\varepsilon^2}\mathrm{Diag}(e^{\mathbf{y}})\mathbf{D}^t(\mathbf{g} - \mathbf{D}\mathbf{y}) = 0,$$

where $\mathrm{Diag}(e^{\mathbf{y}})$ is a diagonal matrix with diagonal entries $(e^{\mathbf{y}})_i$ and $\mathbf{f} = \exp[\mathbf{y}] - \gamma\mathbf{1}$.

Using an M-estimator in the noise model, we replace the loss function $[(g_i - (\mathbf{D}\mathbf{f})_i/\sigma_\varepsilon]$ by $\rho([(g_i - (\mathbf{D}\mathbf{f})_i/\sigma_\varepsilon])$, where $\rho(x)$ has been defined in equation (10).

Let ψ denote the derivative of ρ. For our choice $\psi(x) = x$ for $|x| \leq 2$, and $\psi(x) = 2\,\mathrm{sgn}(x)$ for $|x| > 2$. The robust MAP estimator of $\mathbf{y}$ satisfies

$$\mathbf{y} = \mathrm{Diag}(\omega_{\mathbf{y}})\mathbf{C}\mathbf{y} + (\mathbf{I} - \mathrm{Diag}(\omega_{\mathbf{y}}))\{\mathbf{y} + \mathbf{D}^t[\frac{1}{\sigma_\varepsilon}\psi((\mathbf{g} - \mathbf{D}\mathbf{f})/\sigma_\varepsilon)]\}, \tag{20}$$

where $\mathrm{Diag}(\omega_{\mathbf{y}})$ is a diagonal matrix with diagonal entries $1/(1+\sigma_{\mathbf{y}}^2 e^{\mathbf{y}_i})$. The above equation can be used in an iterative scheme with relaxation for obtaining an estimate of $\mathbf{y}$. This model will be noted LCARN (Logarithmic scale, C.A.R. prior and Normal noise).

5.4 Log scale C.A.R. and Poisson Noise

Let us now assume that we want to impose smoothness constraints on the solution of (15) by using a C.A.R. prior model on log scale, we have

$$p(\mathbf{y}|\mathbf{g}) \propto \exp[-\frac{1}{2\sigma_{\mathbf{y}}^2}\mathbf{y}^t(\mathbf{I} - \mathbf{C})\mathbf{y}] \prod_{i=1}^{p} \exp\left[-(\mathbf{D}\mathbf{f})_i\right][(\mathbf{D}\mathbf{f})_i]^{\mathbf{g}_i}/\mathbf{g}_i! \tag{21}$$

Differentiating $-\log p(\mathbf{y}|\mathbf{g})$ with respect to $\mathbf{y}$ we obtain

$$\frac{1}{\sigma_y^2}(\mathbf{I} - \mathbf{C})\mathbf{y} + \mathrm{Diag}(e^{\mathbf{y}})[\mathbf{1} - \mathbf{D}^t(\mathbf{g}/\mathbf{D}\mathbf{f})] = 0$$

or

$$\mathbf{y} + \sigma_{\mathbf{y}}^2 \mathrm{Diag}(e^{\mathbf{y}})\mathbf{1} = \mathbf{Cf} + \sigma_{\mathbf{y}}^2 \mathrm{Diag}(e^{\mathbf{y}})\mathbf{D}^t(\mathbf{g}/\mathbf{Df}) \tag{22}$$

multiplying, component wise, both sides of (22) by $\mathbf{y}$ we obtain

$$\mathbf{y} = \mathrm{Diag}(\omega_{\mathbf{y}})\mathbf{Cy} + (\mathbf{I} - \mathrm{Diag}(\omega_y))\mathrm{Diag}(\mathbf{y})\mathbf{D}^t(\mathbf{g}/\mathbf{Df}) \tag{23}$$

where $\mathrm{Diag}(\omega_{\mathbf{y}})$ is a diagonal matrix with diagonal entries $\mathbf{y}_i/(\mathbf{y}_i + \sigma_{\mathbf{y}}^2 e^{\mathbf{y}_i})$.

The above equation can be used in an iterative scheme with relaxation for obtaining an estimate of $\mathbf{y}$. This model will be noted LCARP (Logarithmic scale, C.A.R. prior and Poisson noise).

6 An astronomical application

The impact of comet Shoemaker-Levy 9 with Jupiter was the first collision between two bodies in the Solar System that has been predicted in advance. The images presented here were acquired using a CCD camera at the William Herschel Telescope trough two narrow-band interference filters centered at the methane band at 892 nm and its adjacent continuum at 948 nm on July 18th, 1994. They show clearly the effect of impacts H (near the central meridian), and complex D/G (close to the limb). These impacts appear as bright features in the methane filter, and dark ones in the continuum one. A detailed description of the observation and data reduction is shown in [15]. Figure 1 and figure 2 show the original images as well as the resulting images after the application of the different deconvolution approaches. In figure 3 it is shown a contour map of the 892 nm image with two cuts which will be used to make a comparison of the methods. In general, all the four methods give acceptable results, except the CARN method, that produces excessive ringing around high-contrast, rapidly-varying intensity features. However, it produces more contrast than the other methods do on more subtle features. This is illustrated in figures 4 – 6. Figure 4 shows a cut along the x axis of the frame at the position of the jovian satellite close to the planet pole. The satellite is a very bright feature in the methane images, as it does not have a considerable atmosphere. It is seen how the CARN method (solid line) produces ringing around the satellite, even producing a negative count level below zero, which is physically unrealistic. It also produces a wrong satellite profile, by enhancing too much the phase curve. The same feature is found in the LCARP method (both dotted and dashed line). For these high-contrast features, the best suited models are LCARN (dashed line) and CARP (dotted line), which produce better contrast images without modifying the profile close to the maximum intensity or the wings of the profile. In figure 5, in which a cut across the Great Red Spot, the H-impact site and the south polar hood at 892 nm is represented, there is more subtle differences among the profiles for the different restoration methods. Only at the H-site and at the limb of the planet the differences are enhanced, because these features are also of very high contrast. In the continuum images (see figure 6), there is essentially no differences among the profiles, although the LCARP model gives the highest contrast images.

Acknowledgements

The 4.2-m William Herschel Telescope is operated on the island of La Palma by the Royal Greenwich Observatory in the Spanish Observatorio del Roque de los Muchachos of the Instituto de Astrofísica de Canarias.

The work of R. Molina, J. Mateos, J. Abad and N. Pérez de la Blanca has been supported by the "Comisión Nacional de Ciencia y Tecnología" under contract PB93-1110. The work of A. Molina and F. Moreno has been supported by the Comisión Nacional de Ciencia y Tecnología under contracts ESP94-0719, ESP94-0803 and ESP93-0338.

References

1. S.F. Gull, "Developments in Maximum Entropy Data Analysis," in *J. Skilling (Ed). Maximum Entropy and Bayesian Methods, Cambridge*, Kluwer Academic Press, pp. 53-71, 1989.

2. S.F. Gull and J. Skilling "MEMSYS 5 Users's Manual". Maximum Entropy Consultants Ltd., 1991.

3. N. Weir "Recent Developments in Maximum Entropy Based Image Restoration," *ST-ECF Newsl.*, vol. 16, pp 8-11, 1991.

4. L.B. Lucy, "An Iterative Technique for the Rectification of Observed Distributions," *Astron. J.*, vol. 79, 745-754, 1974.

5. J. Llacer and J. Núñez, "Iterative Maximum Likelihood Estimator and Bayesian Algorithms for Image reconstruction in Astronomy," in *R.L. White and R.J. Allen (Eds). The Restoration of HST Images and Spectra.* STScI, Baltimore, pp. 62-70, 1990.

6. H.M. Adorf, "HST Image Restoration. Status and Prospects," in *V. Di Gesù, L. Scarsi, R. Buccheri, P. Crane, M.C. Maccarone and H.U. Zimmermann (Eds). Data Analysis in Astronomy, Vol IV*, Plenum Press. pp 83-96, 1992.

7. R.L. White and R.J. Allen, (Eds). *Proc. Workshop "The Restoration of HST Images and Spectra."*. Space Telescope Science Institute, Baltimore 21-22 August 1990.

8. R.J. Hanisch and R.L. White, (Eds). *Proc. Workshop "The Restoration of HST Images and Spectra II."*. Space Telescope Science Institute, Baltimore 18-19 November 1993.

9. Richardson, W.H. "Bayesian-based Iterative Methods of Image Restoration," *J. Opt. Soc. Am.*, vol. 62, pp 52-55, 1972.

10. R. Molina and B.D. Ripley, "Using Spatial Models as Priors in Astronomical Images Analysis," *J. Appl. Statist.*, vol. 16, pp. 193-206, 1989.

11. J. Núñez and J. Llacer "HST Image Restoration with Variable Resolution," in *R.J. Hanisch and R.L. White (Eds). The Restoration of HST Images and Spectra II.* STScI, Baltimore, pp. 123-130, 1993.

12. B.D. Ripley, *Spatial Statistics.* John Wiley, pp. 88-90, 1981.

13. R. Molina, B.D. Ripley, A. Molina , F. Moreno and J.L. Ortiz, "Bayesian Deconvolution with Prior Knowledge of Object Location. Applications to Ground-Based Planetary Images," *Astrom. J.*, vol. 104, pp. 1662-1668, 1992.

14. R. Molina, A. del Olmo, J. Perea and B.D. Ripley, "Bayesian Deconvolution in Optical Astronomy," *Astrom. J.* , vol. 103, pp. 666-675, 1992.

15. F. Moreno, O. Muñoz, A. Molina, J.J. López-Moreno, J.L. Ortiz, J. Rodríguez, A. López-Jiménez, F. Girela, S.M. Larson, and H. Campins. "Physical properties of the aerosol debris generated by the impact of fragment H of comet P/Shoemaker-Levy 9 on Jupiter". *Geophys. Res. Letters*, in press, 1995.

FIGURE CAPTIONS

Figure 1. From left to right and top to bottom. (a) Original image at the methane band at 948 nm . (b) Restoration with a CARN model. (c) Restoration with a LCARN model. (d) Restoration with a CARP model. (e) Restoration with a LCARP model.

Figure 2. From left to right and top to bottom. (a) Original image at the methane band at 892 nm . (b) Restoration with a CARN model. (c) Restoration with a LCARN. model. (d) Restoration with an CARP model. (e) Restoration with a LCARP model.

Figure 3.Contour map of the 892 nm image with two sections which will be used to compare the methods.

Figure 4. Cut along the x axis of the of the 892 nm frame at the position of the jovian satellite close to the planet pole. See text.

Figure 5. (Left) Cut across the Great Red Spot, the H-impact site and the south polar hood at 892 nm. (Right) A detail of the H-impact. See text.

Figure 6. (Left) Cut across the Great Red Spot, the H-impact site and the south polar hood at 948 nm. (Right) A detail of the left part image. See text.

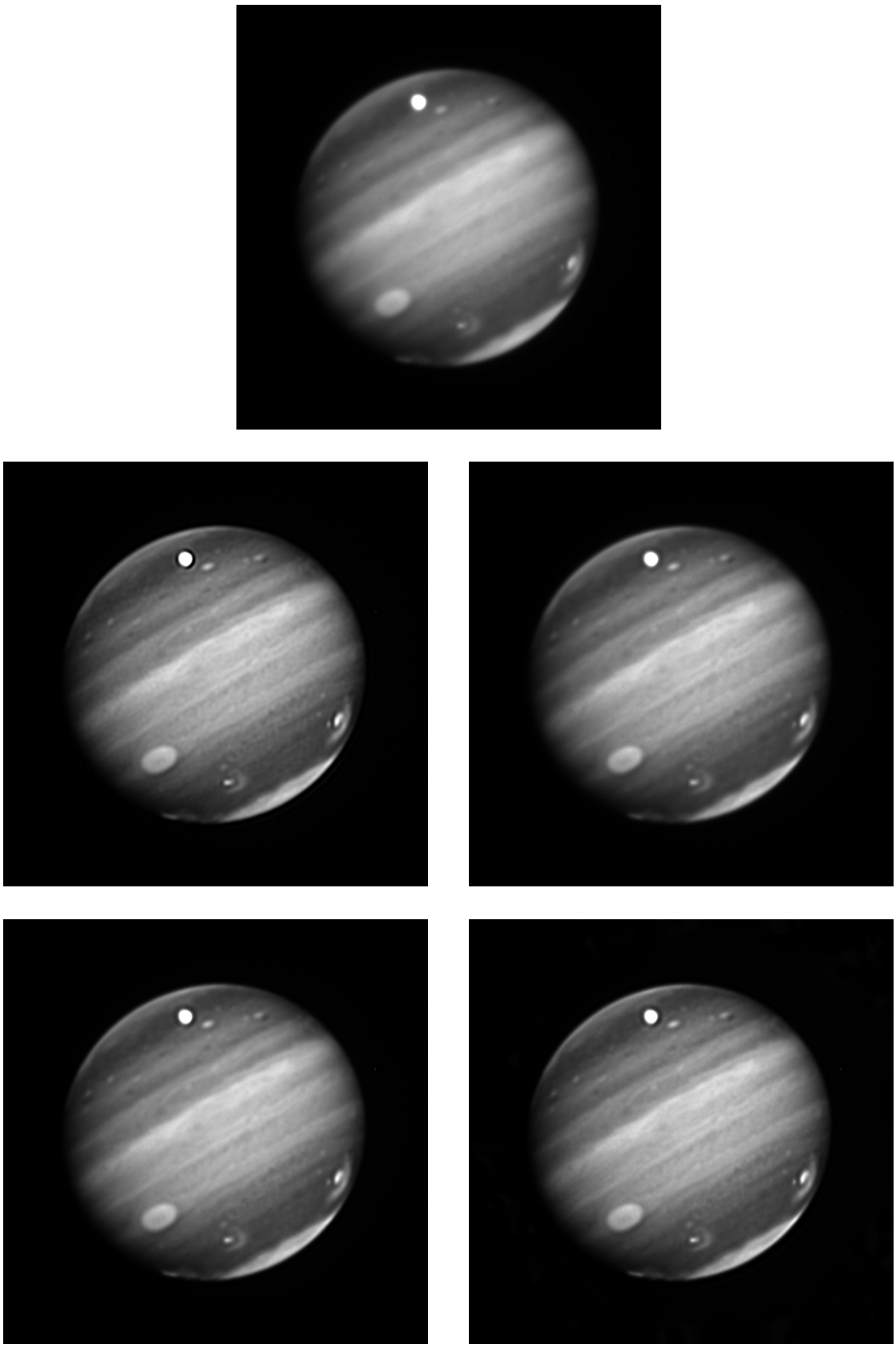

Figure 1:

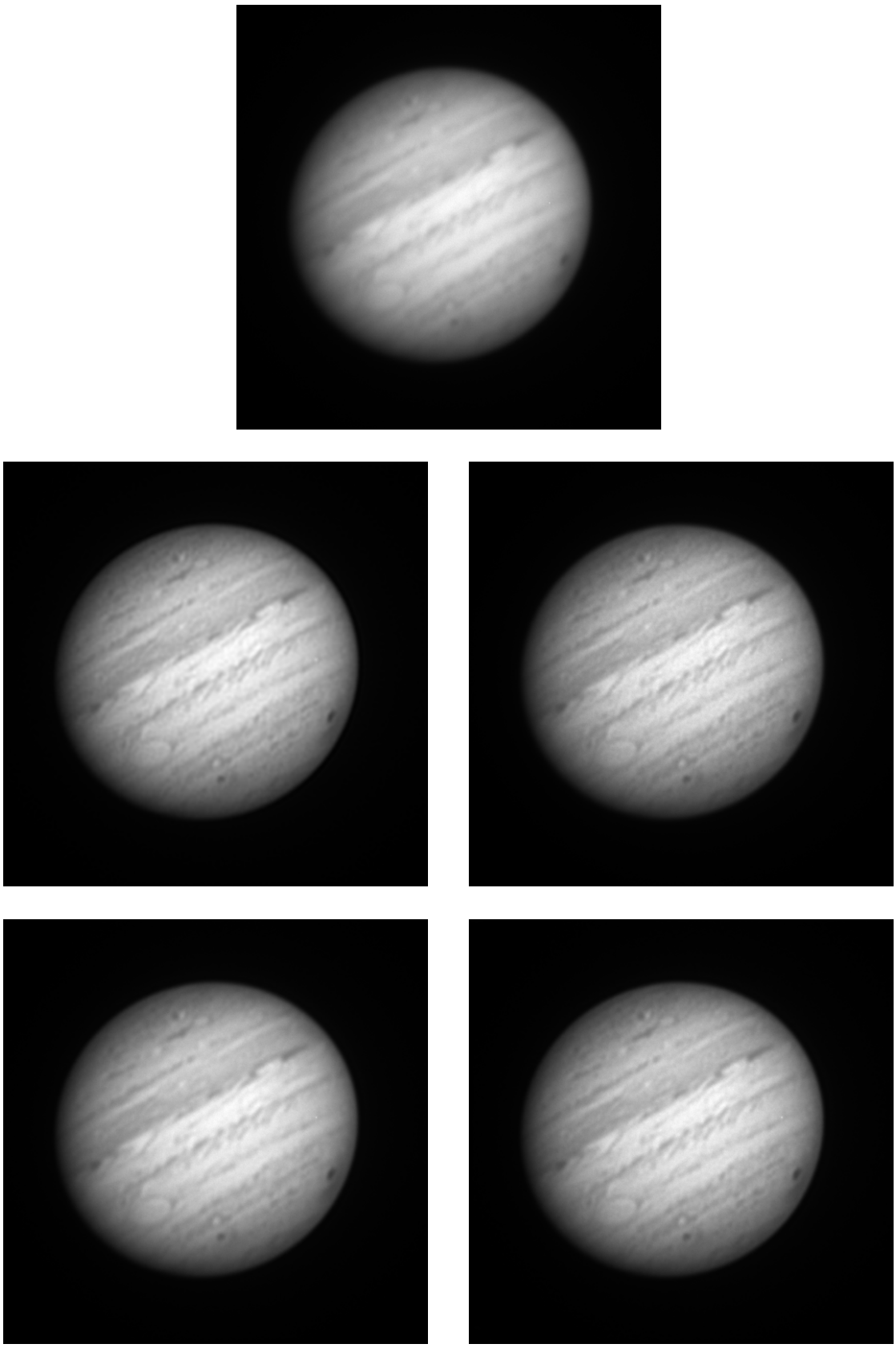

Figure 2:

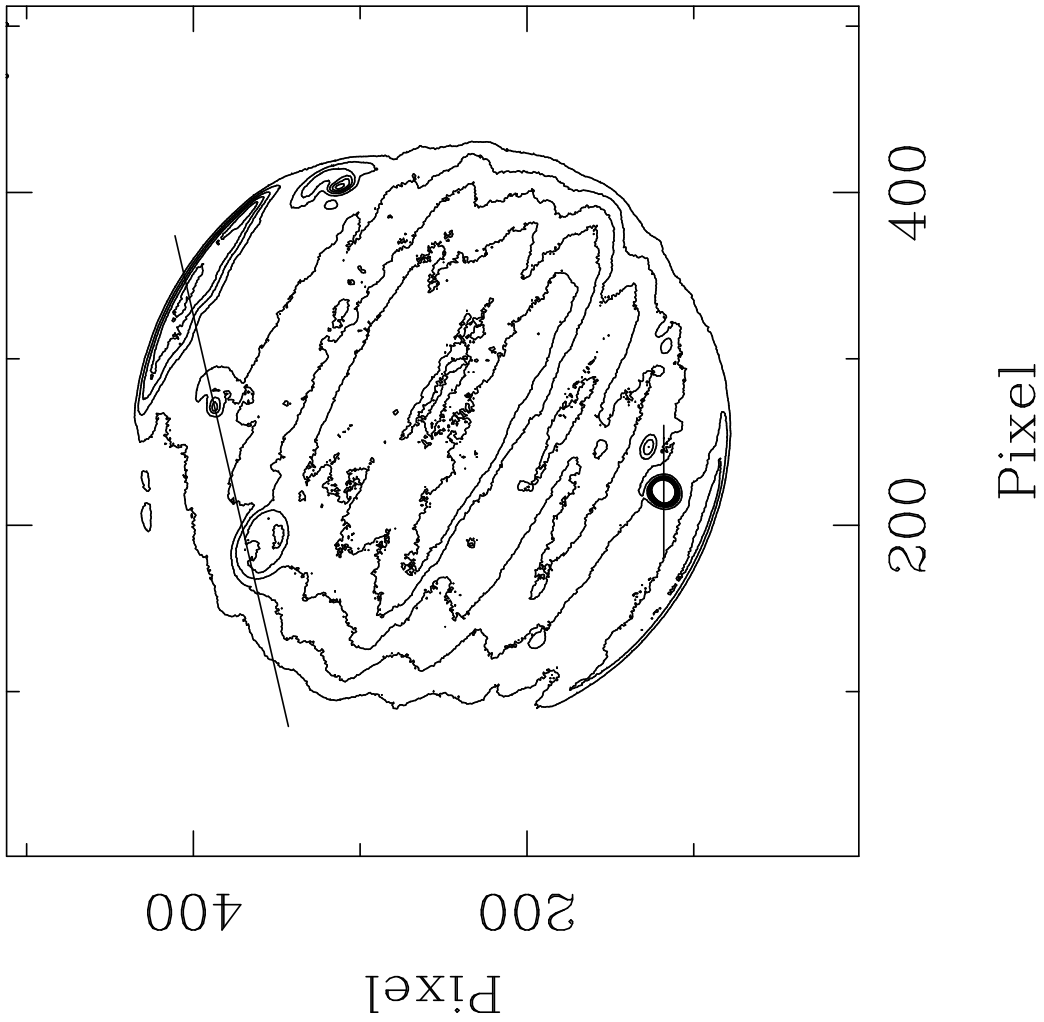

Figure 3:

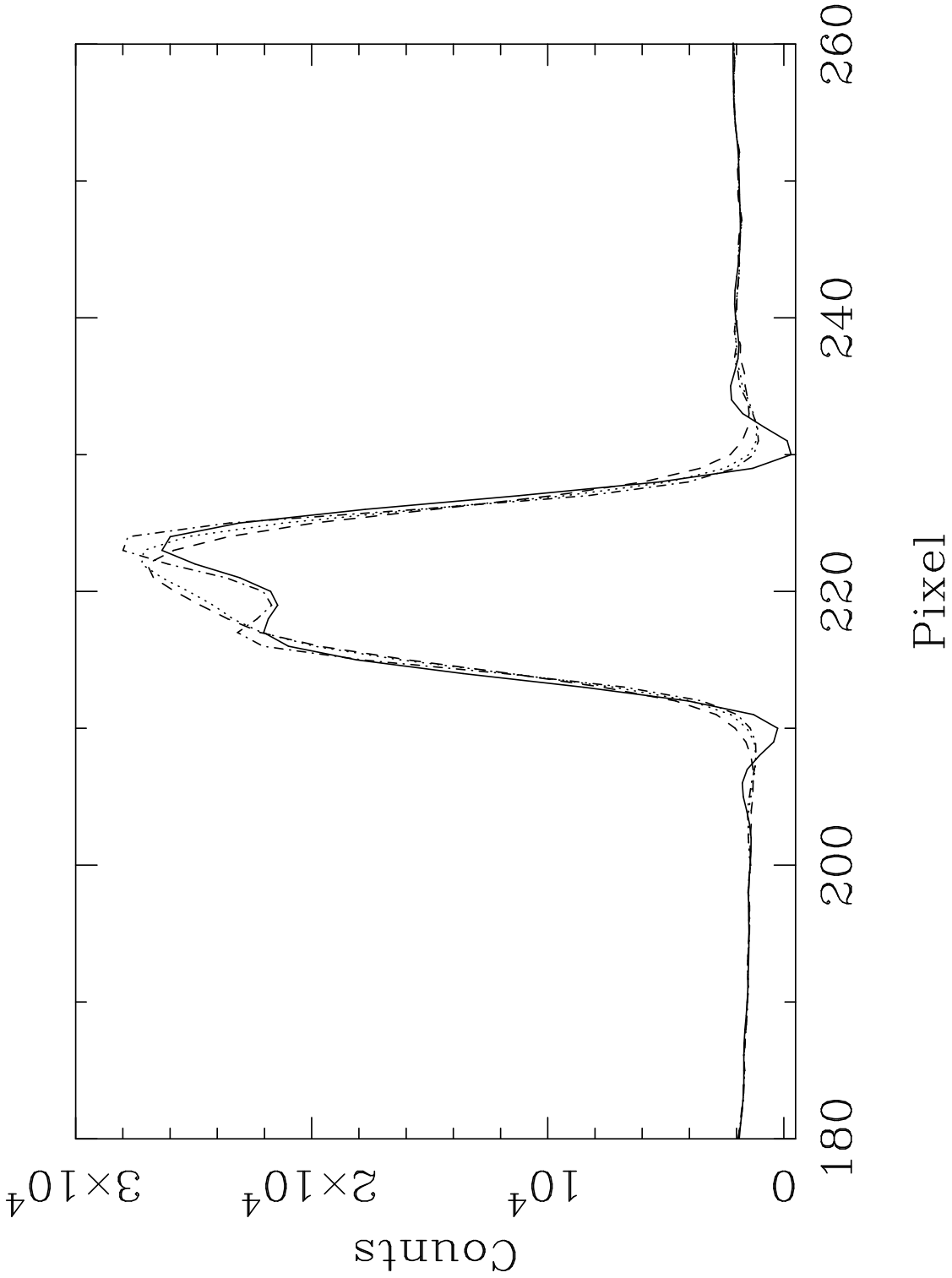

Figure 4:

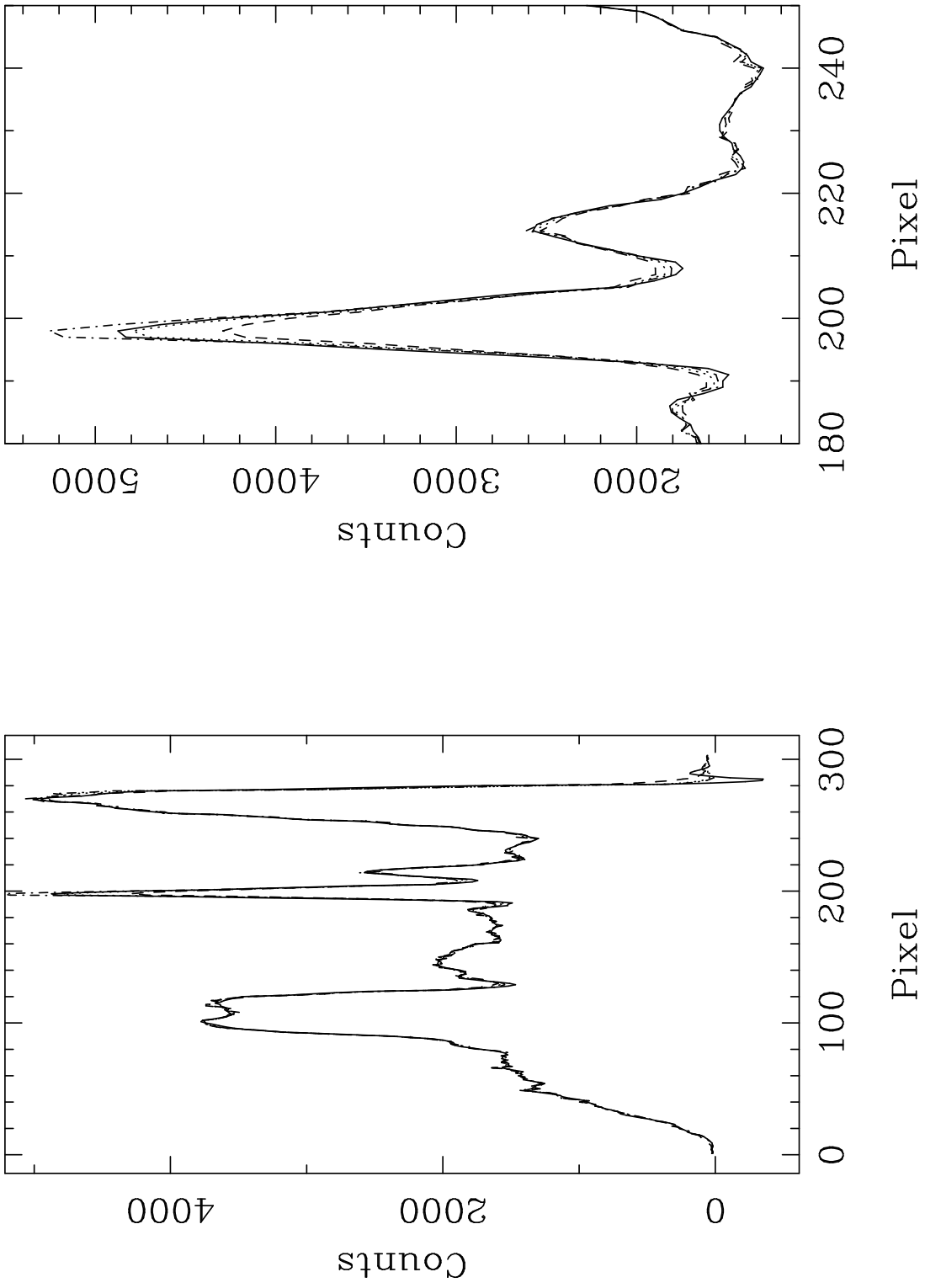
Counts
2000
3000
4000
5000
Pixel
180
200
220
240
Counts
0
2000
4000
Pixel
0
100
200
300

Figure 5:

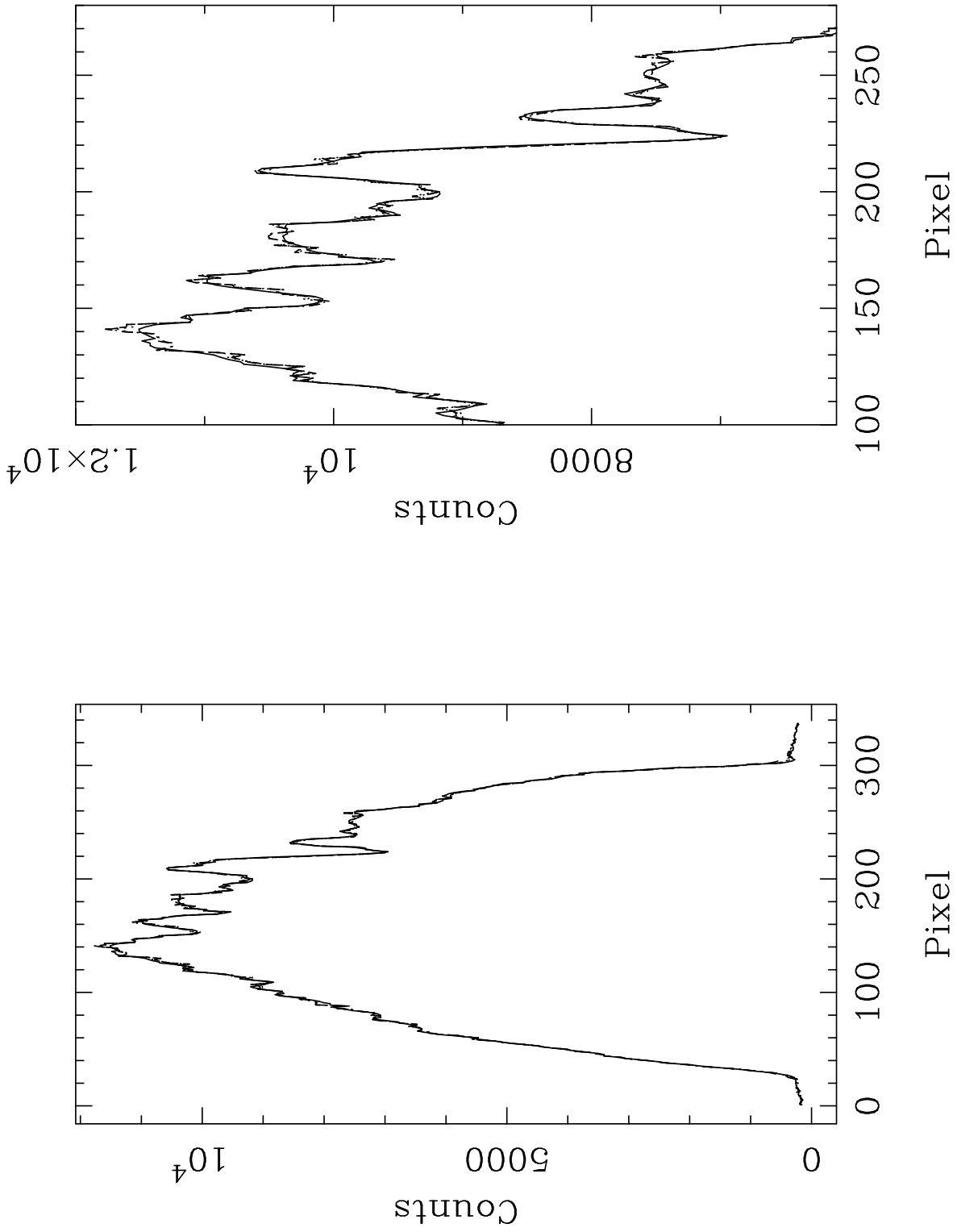
Counts
8000
10^4
1.2×10^4
100
150
200
250
Pixel
Counts
0
5000
10^4
0
100
200
300
Pixel

Figure 6: